MultiCraft

International Journal of Engineering, Science and Technology
Vol. 2, No. 8, 2010, pp. 40-52

INTERNATIONAL JOURNAL OF ENGINEERING, SCIENCE AND TECHNOLOGY

www.ijest-ng.com

Structure, ac conductivity and complex impedance study of Co_3O_4 and Fe_3O_4 mixed spinel ferrites

R.N. Bhowmik, and N. Naresh

Department of Physics, Pondicherry University, R..Venkataraman Nagar, Kalapet, Puducherry –605014, INDIA.
**E-mail of corresponding author: rnbhowmik.phy@pondiuni.edu.in*

Abstract

We have synthesized the composition of $Fe_{3(1-x)}Co_{3x}O_4$ (x =0.1, 0.3 and 0.5) spinel ferrite using the techniques of mechanical alloying, high temperature annealing of milled samples and conventional solid state sintering. We present here comparative results of the crystal structure formation and dielectric properties of the materials studied at room temperature. The crystalline structure of the single phased samples is cubic spinel phase with space group Fd3m. The alloying of two spinel oxides (i.e., Fe_3O_4 and Fe_3O_4) is also complemented from FTIR spectrum. Impedance spectroscopy suggested only one semi circle in the Cole-Cole plot of mechanical milled samples, which indicated the dominant grain boundary contribution in the conduction mechanism. In addition to the grain boundary contribution, the electrical conduction from grains is also substantial in the single phased compositions of the present material. The present results could be interesting in tailoring the electrical conductivity in magnetic nanocomposite.

Key words: Mechanical alloying, Co doped magnetite, Grain and Grain boundary conduction, Magnetic composite.

1. Introduction

Ferrites belong to a special class of magnetic oxides with formula unit AB_2O_4 (A: tetrahedral sublattice, B: octahedral sublattice). The discovery of novel magnetic (e.g., ferrimagnetism, high Curie point), electric (e.g., metal-insulator transition, colossal magnetoresistance) and dielectric (e.g., high permittivity, dielectric loss, universal scaling of ac conductivity, dipole relaxation) properties have made ferrites more attractive to the current field of science and technology (Miles *et al*., 1957). These properties are largely dependent on the elemental composition, route of material synthesis, synthesis condition (sintering temperature, time, etc), grain size and surface morphology, and heterogeneity in the materials. From application point of view, ferrites have shown multi-functional character and properties that can be tailored for making micro-electric devices, magnetic sensors, magnetic switches, electro-magnetic circuits and microwave devices (Jun Y.-wook *et al.*, 2007). A list of ferrite compounds is already reported in literature (Chicinas, 2006). Those ferrite compounds can be treated as the derivative of magnetite (Fe_3O_4), i.e., $Fe_{3-x}M_xO_4$ with M is the transition elements (Cr, Mn, Co, Ni, Zn, etc). Magnetite (Fe_3O_4) is a typical ferrimagnet with cations distribution $(Fe^{3+})_A[Fe^{2+}Fe^{3+}]_BO_4$ and magnetic moment 4 μB per formula unit. The Curie point (T_C) has been observed at about 850 K. The observation of an unconventional Verwey transition at 120 K in magnetite is believed due to the change of crystal symmetry from cubic to monoclinic structure and charge–orbital ordering (Huang *et al*., 2006). Magnetite is electrically a good conductor at room temperature and above. On decreasing temperature, the insulating (semi-conducting) character of magnetite changed into metallic state, marking a metal-insulator transition near to Verwey transition (Garc´ıa and Sub´ıas, 2004). These experimental results clearly indicate that there is a strong correlation between structure, magnetism and electrical conduction in Fe_3O_4. At the other end, Co_3O_4 is a typical antiferromagnet with Neel temperature below 30 K and electrically semiconductor/insulator.

Transition metal doped magnetite has become an ingredient in the formation of metallic/magnetic nano-composites due to the observations of a wide range of magnetic, electric and other novel properties in its derivatives. For example the study of Co doped Fe_3O_4 series (i.e., $Fe_{3-x}Co_xO_4$ with cation distribution $(Co^{2+}{}_{1-x}Fe^{3+}x)[Co^{2+}{}_x\ Fe^{3+}{}_{2-x}]O_4$) is extremely relevant for describing the mechanism of cation inversion in spinel lattices, tailoring of electrical conductivity from metallic to semiconductor regime (Jonker

et al., 1959; Wang *et al*., 2006), modified ferrimagnetism (Chicinas, 2006; Ramos *et al*., 2007). Another interesting aspect of studying the Co-doped series is the manipulation of magnetic transition temperature and anisotropy in spinel ferrites (Franco *et al*., 2008). This is evidenced from the fact that ferrite nanoparticles in general exhibit superparamagnetic blocking temperature below 300 K, but $CoFe_2O_4$ particles in many cases exhibited blocking temperature well above of 300 K (room temperature). Magnetic crystalline anisotropy of $CoFe_2O_4$ particle is also larger (380 KJ/m^3) (Virden *et al*., 2007) than Fe_3O_4 (14 KJ/m^3) (Fannin *et al*., 2007). In addition to magnetic study the doping effect of Co in Fe_3O_4 lattices can be realized from the study of electrical ac conductivity and dielectric properties. The ac conductivity of ferrites gives valuable information related to the localization of charge carriers at grain and grain boundaries, inter-granular tunneling of charge carriers across the grain boundary and dielectric polarization of magnetic ions. Some reports on electric and dielectric properties are available for Fe_3O_4 derived compounds, such as $CoFe_2O_4$ (Sivakumar *et al*., 2007), $MnFe_2O_4$ (Gopalan *et al*., 2008). The effect of in-homogeneity on the structural, magnetic and electrical properties is not systematically studied for Co^{2+} doped magnetite ($Co_xFe_{3-x}O_4$), although few reports are available (Franco *et al*., 2008; Kim *et al*., 2006).

We have taken a broad research program to examine the structural, electrical, magnetic and dielectric properties of $Fe_{3(1-x)}Co_{3x}O_4$ series in a wide range of Co content. Our objective is not only to synthesize the compound, but also to study the effect of two coexisting Fe_3O_4 and Co_3O_4 cubic spinels or dispersion of Co_3O_4 particles in the matrix of Fe_3O_4 and vice versa. Study of these materials will provide useful information for understanding the mechanism of many recent phenomena, e.g., bio-magnetism, low field magnetoresistance, multiferroelectricity, and grain size and grain boundary controlled electro-magnetic properties (Jun Y.-wook *et al*., 2007; Wang *et al*., 2006). In the present work we have prepared the samples with composition $Fe_{2.7}Co_{0.3}O_4$ (x = 0.1), $Fe_{2.1}Co_{0.9}O_4$ (x= 0.3) and $Fe_{1.5}Co_{1.5}O_4$ (x = 0.5) in three different techniques (mechanical alloying, annealing of the mechanical alloyed powder at highest temperature 950^{0}C and solid state sintering). We maintained identical conditions during materials synthesis for all compositions. We demonstrate mainly the structural phase stabilization, materials characterization and preliminary ac conductivity and dielectric studies at room temperature of the synthesized materials.

2. Experimental Procedure

2.1. Sample Preparation

In mechanical alloying technique, the stoichiometric amount of high purity Fe_3O_4 and Co_3O_4 were mixed to obtain the $Fe_{3(1-x)}Co_{3x}O_4$ composition (x = 0.1, 0.3 and 0.5). The mixture was manually ground using mortar and pestle for 2 hours. The mixed powder was taken into a Silicon Nitride bowl (45 ml). In addition to the material, 10 Silicon Nitrite (10 mm diameter) balls and 10 Tungsten Carbide (5 mm diameter) balls were taken into the bowl. The ball to material mass ratio was maintained to 6:1. The mixed powder was subjected to mechanical alloying using Fritsch Planetary Micro Mill P7 (Germany) in air. The milling was continued at rotational speed 300 rpm up to 24 hours. The option was used for reversing the direction after two hours milling and the milling was stopped for every 4 to 5 hours interval for proper mixing of the alloyed powder, and to minimize the local heat generation and particle agglomeration during material synthesis. Main purpose of the mechanical milling was to form a homogeneous mixture of two spinel oxides Fe_3O_4 and Co_3O_4 with selected molar ratio. We expected that the milling process may form an alloy of complete or partial single phase ferrite through the diffusion of two ferrite grains at the boundaries. The final product even may be the mixture of two ferrites at the grain boundaries. After 24 hours milling, the material of each composition was made into several pellets of 13 mm diameter by applying 2-3 tons pressure. The pellet form of 24 hours milled material is denoted as M1, M3 and M5 for x = 0.1, 0.3 and 0.5, respectively. The remaining pellets of the as milled samples were annealed at 800^{0}C for 6 hours and cooled afterwards to room temperature. From XRD spectrum we noted that single cubic spinel phase is not properly formed for all compositions. The pellets were, further annealed at 950^{0}C for 12 hours. We denoted 950^{0}C annealed samples as A1, A3 and A5 for x = 0.1, 0.3 and 0.5, respectively, and these annealed samples were used for electrical and dielectric studies. In solid state sintering route, the stoichiometric mixture of high purity Fe_3O_4 and Co_3O_4 powders was taken to obtain the $Fe_{3(1-x)}Co_{3x}O_4$ composition. The mixed powder was ground using mortar and pestle for 2 hours and made into pellets. The pre-sintering was done at 1000^{o}C for 12 hour. The pre-sintered mixture was ground and pressed at 5 tons pressure into a disk of 13 mm diameter. Finally, the pellet form of the (pre-sintered) samples were sintered at 1100^{o}C for 14 hours and cooled down to room temperature with controlled rate of 4^{o}C/min. The solid state sintered materials are denoted as B1, B3 and B5 for the composition x = 0.1, 0.3, 0.5, respectively.

2.2. Sample characterization

Structural phase of the synthesized samples were examined from X-ray diffraction (XRD) spectrum at 300 K (room temperature). The spectrum of each sample was recorded in the 2θ range 10 to 90 with step size 0.02^o using Cu Kα radiation from X-Pert PANalytical diffractometer. Surface morphology of the samples was studied using scanning electron microscope (SEM) (model: HITACHI S-3400N, Japan). Elemental analysis of the samples was carried out using energy dispersive analysis of X-ray (EDX) spectrometer (Thermo electron corporation Instrument, USA). Fourier Transform Infrared Spectroscopy (FTIR) measurement of the samples was performed in the wave number range 400–4000 cm^{-1} using the model Nicolet-6700 (Thermo electron Corporation). Before recording the FTIR spectrum of the studied samples, the instrument was calibrated using standard KBr pellet. The KBr powder was well ground using agate mortar and pestle to reduce the scattering of infrared beam. The grinding

was continued until crystallites can no longer be seen and the powder became somewhat pasty and sticks to the mortar. Then, the fine powder was collected and a small amount of ferrite powdered sample (about 0.1 % of the KBr powder, or just enough to maintain the good transparency of the final pellet) mix with the KBr powder. Subsequently, the mixed powder (ferrite+ KBr) was ground for 5 minutes to make it homogeneous and the ferrite particles be dispersed properly in the mixture. The powder was added to the collar of diameter 3 mm. A transparent pellet of the powder with 3 mm diameter and thickness less than 0.5 mm was made using a Qwik Handi-Press. The collar together with the pellet was put under 100 W bulb for 5 minutes to reduce the moisture content and then put onto the sample holder for FTIR study. AC conductivity and dielectric properties of the samples were measured at room temperature using Broadband Dielectric Spectrometer (Novocontrol technologies, Germany) in the frequency range 1 Hz to 1 MHz at ac electric signal 1 volt. For dielectric measurement, pellet shaped samples were used and sand witched between two gold coated plates, which are connected to the spectrometer with special cables. The as milled (pellet) samples were heated at 200^0C for 2 hours to make it little bit hard before placing the sample in dielectric measurement cell.

3. Results and Discussion

3.1. Structural and morphological study

Figure 1 shows the XRD spectra of milled (M1, M3, M5), annealed (A1, A3, A5) and bulk (B1, B3, B5) samples of $Fe_{3(1-x)}Co_{3x}O_4$ compositions (x =0.1, 0.3, and 0.5). The XRD spectrum was recorded in the 2θ range ~ $10\text{-}90^0$, but data in Figure 1 have been shown in the 2θ range ~ $26\text{-}40^0$ in order to clearly demonstrate the appearance of any additional phase or minor phase at different stages of the sample preparation. The XRD pattern of the milled samples (M_1, M_3, and M_5) shows that Fe_3O_4 and Co_3O_4 phases is not completely alloyed to form the single phased $Fe_{3(1-x)}Co_{3x}O_4$ compound. XRD pattern is found to be the mixture of the proportionate peak intensities from Fe_3O_4 and Co_3O_4 phases, as indicated in the Figure 1.

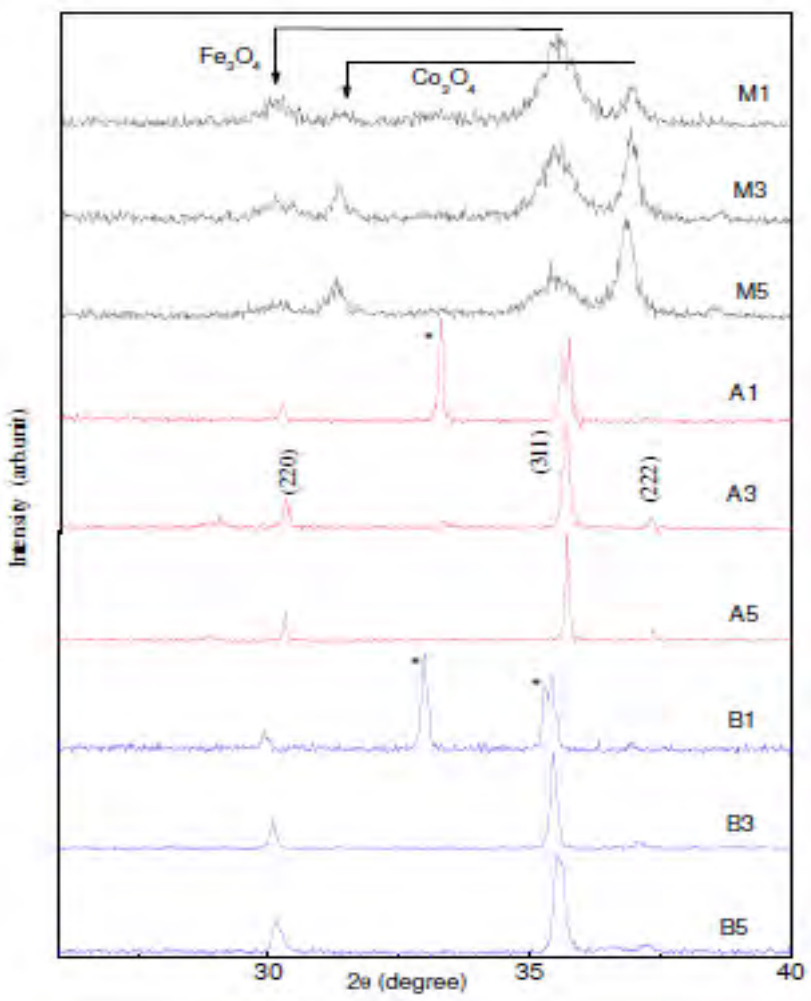

Figure 1. (Colour online) XRD spectrum of $Fe_{3\,(1-X)}\,Co_{3x}O_4$ ferrite composites with x = 0.1, 0.3, and 0.5 in milled (M), annealed (A) and bulk (B) conditions (* represents unreacted α-Fe_2O_3)

This is the expected intensity variation for $Fe_{3(1-x)}Co_{3x}O_4$ composition depending on the value of Co content (x = 0.1,0.3 and 0.5). There is a signature of partial alloying for x=0.3 and 0.5 composition. By annealing the as milled samples at 800^0C for 6 hours, we noted that x = 0.1 composition is not single phased. A minor trace of α-Fe_2O_3 (hematite) phase was observed in x = 0.1 composition, in addition to the cubic spinel phase. Chemical routed samples also exhibited similar additional phase for lower value of Co content in $Fe_{3-x}Co_xO_4$ compound (Franco *et al*., 2008). On the other hand, x = 0.3 and 0.5 compositions showed the signature of single phased compound. To improve the single phased crystalline structure, we annealed the as milled samples at 950^0C for 12 hours (i.e., A1, A3 and A5 samples). XRD spectrum shows that hematite phase (near to $2\theta \sim 33.27^0$ due to strongest (104) peak of rhombohedral crystal structure with space group R3C) is coexisting with cubic spinel structure not only in A1 sample alone, but also in bulk B1 sample (synthesized through solid state sintering route where material was heated at 1100^0C for 12 hours). This experimental result indicate that formation of single phased $Fe_{3(1-x)}Co_{3x}O_4$ compound starting from the mixture of Fe_3O_4 and Co_3O_4 is not favourable for lower value of Co content (here x = 0.1), irrespective of the mechanical alloying and solid state sintering techniques. We attribute this to the multi-valence state of Co ions (i.e., Co^{2+} and Co^{3+} ions in Co_3O_4 spinel oxide) replacing Fe^{2+} ions in Fe_3O_4 spinel oxide. In general divalent Co compound (e.g., CoO) and trivalent Fe compound (e.g., α-Fe_2O_3 (hematite)) are used as the starting materials to form the single phased Co doped Fe_3O_4 ferrites, which is different from our starting materials. In principle, Co^{2+} ions will prefer to occupy the B sites by replacing Fe^{2+} ions in the Fe rich regime of Co doped Fe_3O_4 ferrites (Kim *et al*., 2006). In the presence of Co^{3+} ions, the charge valence of the compound is not neutralized and a fraction of Fe atoms is coming out of the spinel lattices to form the additional phase (hematite) when the material is synthesized in air atmosphere. We believe that reducing atmosphere may be helpful to stabilize the single phased cubic spinel structure for low Co content compound. Although a signature of hematite phase was indicated near to $2\theta \sim 33.27^0$ for A3 sample, this minor trace of α-Fe_2O_3 phase is not significant in comparison with A1 and B1 samples. Hence, the samples A3, A5, B3 and B5 are well matched to the single phased cubic spinel structure with space group Fd3m. The interesting feature from Figure 1 is that the mixed composition with the low Co content is stabilized in the cubic spinel phase of Fe_3O_4 (i.e., inverse spinel structure) and tending to stabilize in normal spinel structure of C_3O_4 with the increase of Co content in $Fe_{3(1-x)}Co_{3x}O_4$ composition. For higher Co content compound (e.g. x = 0.5), some of the A sites Fe^{3+} ions are replaced by Co^{2+} ions and equal amount of B sites Fe^{2+} ions are replaced by Co^{3+} ions. This structural transformation from inverse spinel (for lower Co content) to normal spinel (for higher Co content) was earlier supported from Mössbauer spectroscopy (Kim *et al*., 2006).

Lattice parameter (*a*) of the $Fe_{3(1-x)}Co_{3x}O_4$ composition (x = 0.1, 0.3 and 0.5) was calculated by matching the XRD spectrum to the cubic spinel structure with space group Fd3m. The lattice parameter (*a*), as shown in Table 1, shows a general tendency to decrease with the increase of Co content. This is, in fact, not a simple effect of the ionic radius of Co ions (~0.67 Å for B site low-spin Co^{3+}, ~0.88 Å for B site high-spin Co^{2+}, ~0.72 Å for A site high-spin Co^{2+}) doped in the lattice sites of Fe ions (ionic radius ~0.78 Å for B site high-spin Fe^{3+}, ~0.92 Å for B site high-spin Fe^{2+}). However, this feature is consistent with the experimental data on $Co_xFe_{3-x}O_4$ (Tseung *et al*., 1972; Kim *et al*., 2006) and related to the site exchange of cations. Interestingly, the lattice parameter of the bulk sample is slightly larger than the annealed samples. This is attributed to the differences in grain size and microstructure of the bulk and annealed samples.

Table. 1 Lattice parameter from cubic spinel phase component of XRD spectrum, absorption peaks from FTIR spectrum, grain resistivity (ρ_g) and grain boundary resistivity (ρ_{gb}) of $Fe_{3(1-x)}Co_{3x}O_4$ ferrite with compositions x = 0.1, 0.3 and 0.5. All the measurements were performed at room temperature.

Sample	Lattice Parameter (A^o)	Absorption peak ν_1 (cm^{-1}) for A site metal-O ion		Absorption peak ν_2 (cm^{-1}) for B site metal-O ion		ρ_g (ohm-cm)	ρ_{gb} (ohm-cm)
M1	-	578	662	457	-	-	$122.46X10^8$
M3	-	580	668	432	-	-	$36.11X10^8$
M5	-	582	670	419	-	-	$52.44X10^8$
A1	8.3812±0.00421	588	-	472	414	-	-
A3	8.3526±0.00418	595	-	464	416	$7.12X10^6$	$25.25X10^7$
A5	8.3290±0.00416	609	-	461	425	$4.41X10^6$	$21.704X10^7$
B1	8.3901±0.0083	557	-	467	-	-	-
B3	8.3887±0.0084	687	-	417	-	$7.32X10^7$	$21.22X10^8$
B5	8.3566±0.0089	598	-	418	-	$17X10^7$	$19.34\ X10^7$

Figure 2 (a-c) shows the SEM pictures of x = 0.5 composition in different stages of sample preparation, i.e., (a) for 24 hours milled sample (M5), (b) for 950^0C annealed sample (A5), and (c) for solid state sintered bulk sample (B5). From SEM picture of M_5 sample (Fig.2a) we noticed that almost 8-10 particles are agglomerated in the scale of 500 nm and exhibited nearly spherical shaped particles with size ~60 nm. This image also suggests interesting points related to the alloying of ferrite particles across the boundary region. Considering the high (ferrimagnetic) moment of Fe_3O_4 particles at room temperature in comparison with the low (paramagnetic) moment of Co_3O_4 particles, we suggest that Co_3O_4 particles are attracted by the Fe_3O_4 particles and attached to the

surface of Fe_3O_4 particles. Hence, the alloy formation in the present work can be due to the reaction of Co_3O_4 particles in the surfaces (or grain boundaries) of Fe_3O_4 particles. By annealing it was noted that there are nearly 3 spherical shaped particles in the length of 2x500 nm for A5 sample, which gives particle size nearly 170 nm. The particles are in contact to each other with a homogeneous distribution over the region. The B5 sample showed the distribution of well crystalline (polygon shaped) particles with dimension 2-3 μm and the microstructure is significantly different from the mechanical alloyed (M5 and A5) samples. Figure 2 (d-f) shows the surface morphology of the distributed particles in different length scale of SEM picture for the x = 0.3 sample sintered at 1000^0C. In the length scale of 20 μm (Figure 2(d)), the particles appeared to be less agglomerated and nearly uniform distribution of particles. On further decreasing the measurement scale to 5 μm (Figure 2(e)) and 500 nm (Figure 2(f)), we are confirmed that the particles are really spherical in shape and instead of agglomeration; the tiny particles are spherical in shape with size ≥ 500 nm. Figure 2(f) confirmed that particle size of the solid state sintered sample is larger than that of the mechanical alloyed sample. In addition to that shape and morphology of the solid state sintered material is drastically changed with the increase of sintering temperature from 1000^0C to 1100^0C. This observation suggests that well crystalline structure of ferrite material occurs above 1000^0C sintering temperature. Similar morphological transformation was noted above 1100^0C for Ho doped $CoFe_2O_4$ spinel ferrite (Muthuselvam *et al.*, 2010). It is worthy to mention that the particle size from SEM pictures is well consistent to the grain size (crystallite size) of the mechanical milled and annealed samples. The grain size was calculated using prominent XRD peaks of the cubic spinel phase and applying Debye-Scherer formula. The grain size was found approximately 50-60 nm and 100-115 nm for milled and 950^0C annealed samples, respectively. The grain size does not depend significantly on the value of x (0.1, 0.3, 0.5). This indicated that particles in mechanical milled samples are nearly single domain (crystallite).

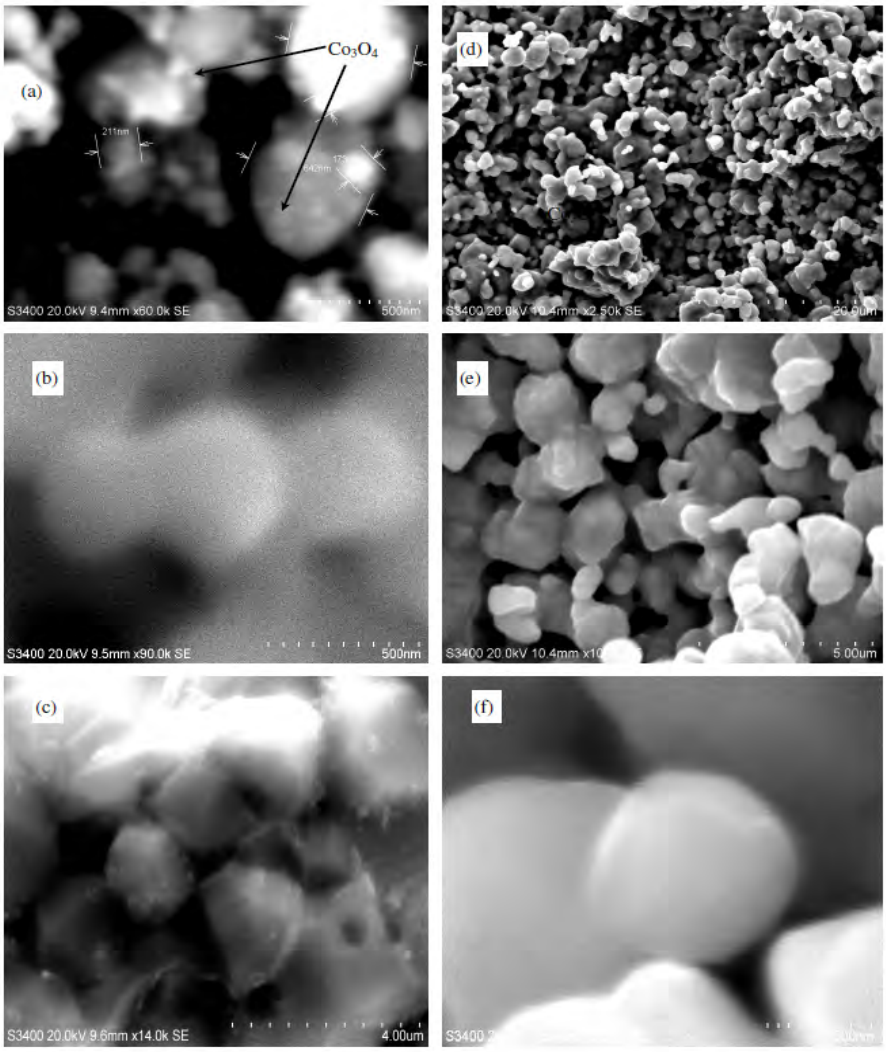

Figure 2. Show the SEM pictures of $Fe_{3(1-x)}Co_{3x}O_4$ ferrite. For x = 0.5, 24 hours milled sample (M5) at 500 nm scale (a), 950^oC annealed sample (A5) at 500 nm scale (b) and 1100^0C sintered bulk sample (B5) at 4μm scale (c) samples. SEM pictures of x = 0.3 bulk sample sintered at 1000^oC with different scale 20 μm (d), 5μm (e) and 500 nm (f), respectively.

A significant difference between particle size (170 nm) and grain size (100-115 nm) in annealed samples is attributed to the multi-grain nature or small agglomeration of nano-grained particles. Agglomeration is possible due to the inter-particle (surface) interactions among ferrite grains with sufficiently strong magnetic moment. The distribution of elements in the synthesized materials was examined using different options of elemental analysis using EDX spectrum. For example, micro point analysis of samples M1 (Figure 3(a)) and B3 (Figure 3(b)) confirmed the presence of main elements Fe, Co and O with atomic ratio as expected for the composition $Fe_{3(1-x)}Co_{3x}O_4$. The impurity contamination (mainly Si and W) from bowl and balls during 24 hours milling is insignificant and less than 0.3 atomic %. The line spectrum of A3 sample (Figure 3(c)) over the scanning length 55 μm suggests that more or less uniformly distributed in the annealed sample. On the other hand, elemental (for Co, Fe, O) mapping over the area 70x60 μm^2 for M1 sample (Figure 3(d-f)) clearly shows elemental in-homogeneity in the 24 hours milled samples.

Figure 4 (a-d) shows the comparative FTIR spectra of starting Fe_3O_4 and Co_3O_4 spinel oxides, mechanical milled (M1, M3, M5), annealed (A1, A2, A5) and bulk (B1, B3, B5) samples. The wave number bands ranging 300-700 cm^{-1} are attributed to the fundamental vibration of metal–oxygen bonds in crystalline solids (Waldron *et al*., 1955). The bands with peak at about 670-545 (ν_1) and 425-400 cm^{-1} (ν_2) are assigned due to the modes of stretching vibrations and bending vibrations of metal-oxygen bonds from tetrahedral and octahedral sites, respectively. The observed prominent band positions (ν_1 and ν_2) of our samples are shown in Table 1. Figure 4(a) shows that the strong absorption peak at about 558 cm^{-1} (ν_1) for inverse spinel Fe_3O_4 is in the range of reported value 550-570 cm^{-1} (Waldron *et al*., 1955). The splitted absorption peaks (ν_1) at about 667 cm^{-1} and 580 cm^{-1} for normal spinel Co_3O_4 are also in the range of reported values 669 cm^{-1} and 578 cm^{-1} (Li *et al*.,2008).

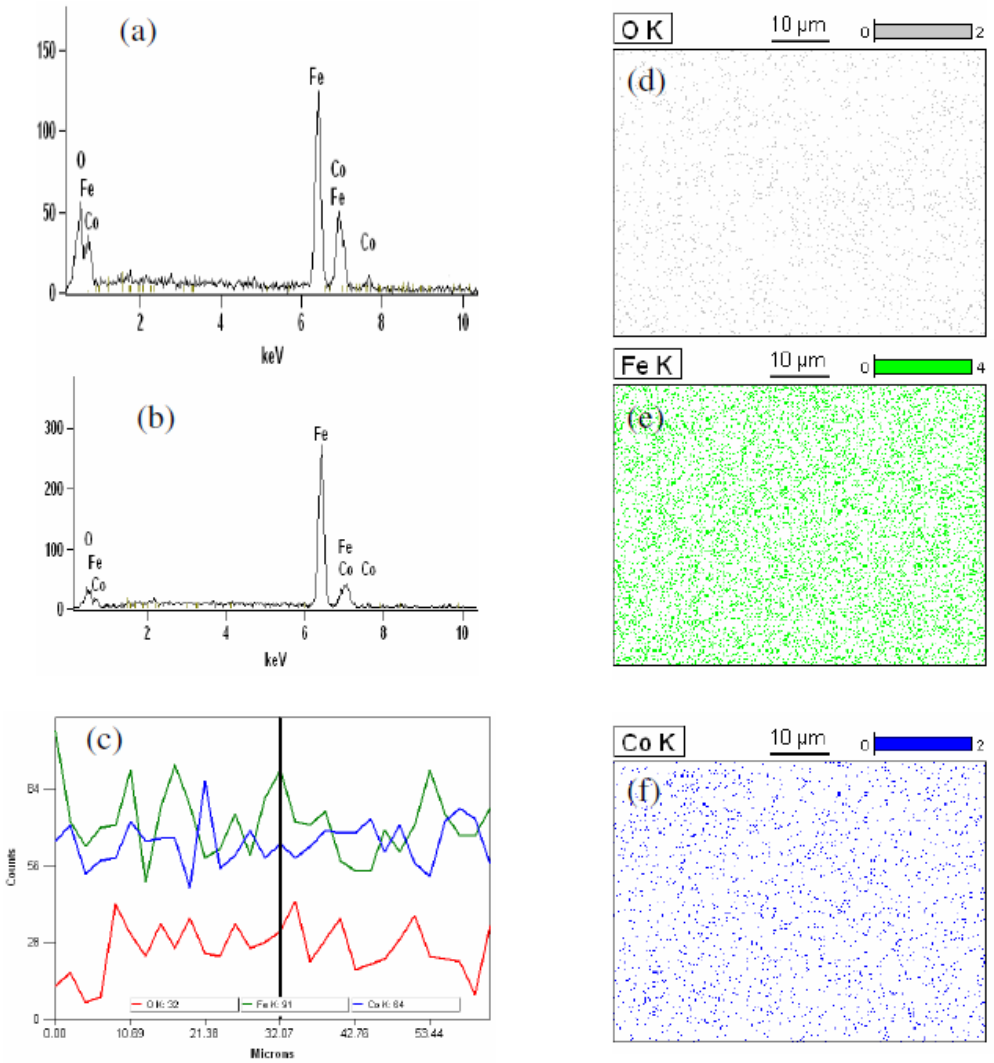

Figure 3. (a)-(b) show the EDX spectra for M1 and B3 samples, respectively. (c) shows the line spectrum for A5 sample. (d)-(f) show the mapping of Oxygen, Iron, Cobalt elements for M1 sample, respectively.

FTIR spectrum (Figure 4 (b-d)) also supports the structural evolution of the samples, as observed from the XRD spectrum. There is a clear trend of increasing peak intensities at about the components of ν_1 peaks of Co_3O_4 with the increase of Co content in the composition $Fe_{3(1-x)}Co_{3x}O_4$. FTIR spectrum suggests that milled samples (M1, M3, M5) are not single phased compound. As an

effect of partial alloying in milled samples, the absorption peaks are shifting from 578 to 582 cm^{-1} and 662 to 670 cm^{-1} for tetrahedral (ν_1) site vibration and 457 to 419 cm^{-1} for octahedral (ν_1) site vibration. Comparing the FTIR spectrum of Fe_3O_4 and Co_3O_4 spinels and noting the appearance of a single peak at about ν_1 band, the present work confirms the doping of Co atoms in the Fe_3O_4 lattices in annealed (Figure 4 (c)) and bulk (Figure 4 (d)) samples. Other significant observations, i.e., shifting of peak positions as shown in Table 1, are reflecting the internal changes from inverse spinel (low Co content) to normal spinel (higher Co content) structure in the compound. The broad peak at about ν_1 band (~ 588 cm^{-1} for A1 sample and ~ 557 cm^{-1} for B1 sample) is attributed to the superposition of absorption peak at about 532.5 cm^{-1} from α-Fe_2O_3 (Li *et al.*, 2009). The coexistence of α-Fe_2O_3 phase in A1 and B1 samples is further supported from the observed strong peaks at about 472 cm^{-1} for A1 sample and at about 467 cm^{-1} for B1 sample, which is affected by the typical peak of α-Fe_2O_3 at 463 cm^{-1}.

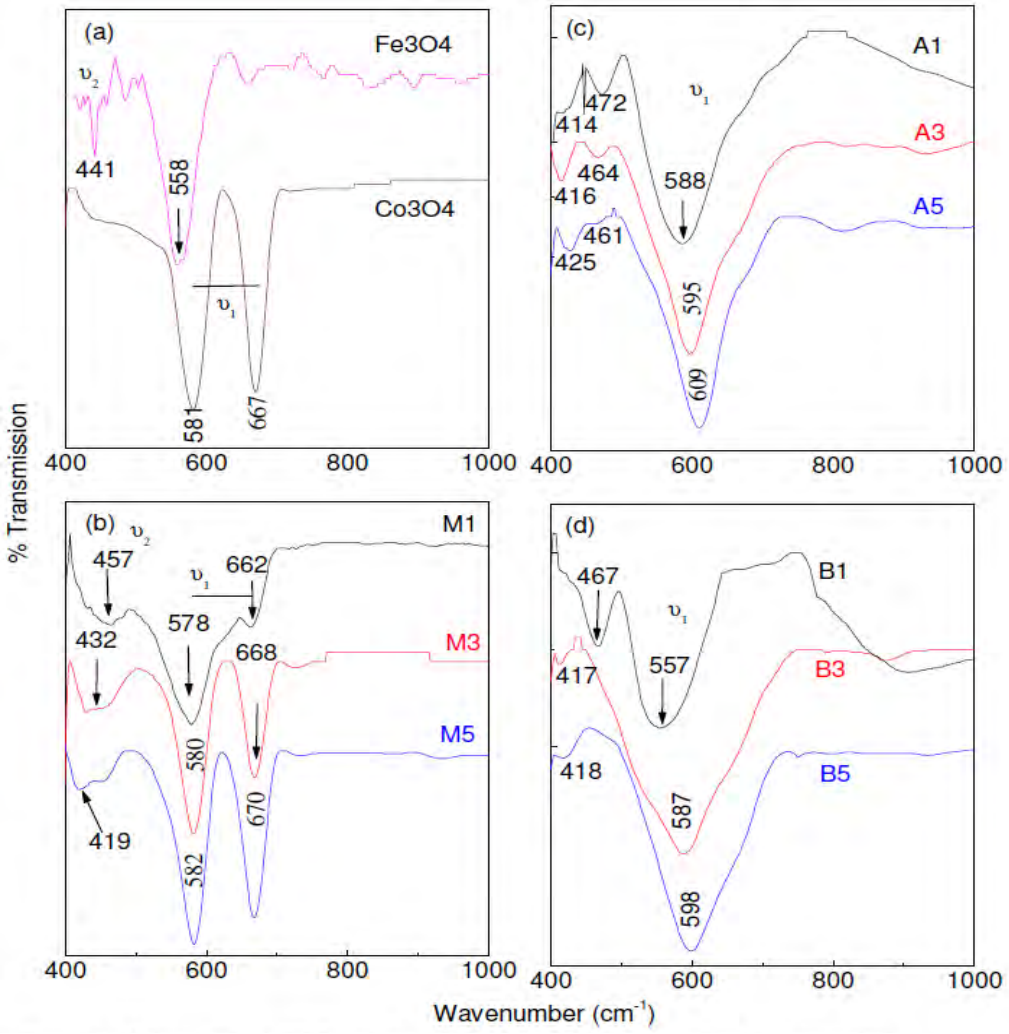

Figure 4. (Colour online) FTIR spectra for $Fe_3O_4$and Co_3O_4 (a), milled (b), annealed (c) and bulk (d) samples. Prominent absorption peaks are indicated by arrows.

3.2. AC conductivity at room temperature

Figure 5 shows the log-log scale plot of the frequency (f) dependence (range: 1 Hz-1MHz) of the variation of ac conductivity (real part: σ', imaginary part: σ'', absolute conductivity: σ) for milled (M1, M3, M5), annealed (A3, A5) and bulk (B3, B5, starting materials Fe_3O_4 and Co_3O_4 spinels). σ' is less frequency dependent (i.e., plateau like response) up to 100 Hz for milled samples. Then, log σ' increases linearly with the increase of frequency (log(f)) that shows a power law behavior. On the other hand, σ'' follows a power law increase in the whole frequency range. The resultant of σ' and σ'', i.e., σ also follows a nice power law behviour in the form of $\sigma \sim f^n$, where n is power exponent. The slow response of conductivity extends to higher frequency value with the increase of Co content in the $Fe_{3(1-x)}Co_{3x}O_4$ composition. Since x = 0.1 composition did not form the single phased compound, detailed ac conductivity and dielectric properties of the A1 and B1 samples are not discussed in this paper. We see that frequency activated ac conductivity of the annealed and bulk samples, which had shown a good signature of single phased

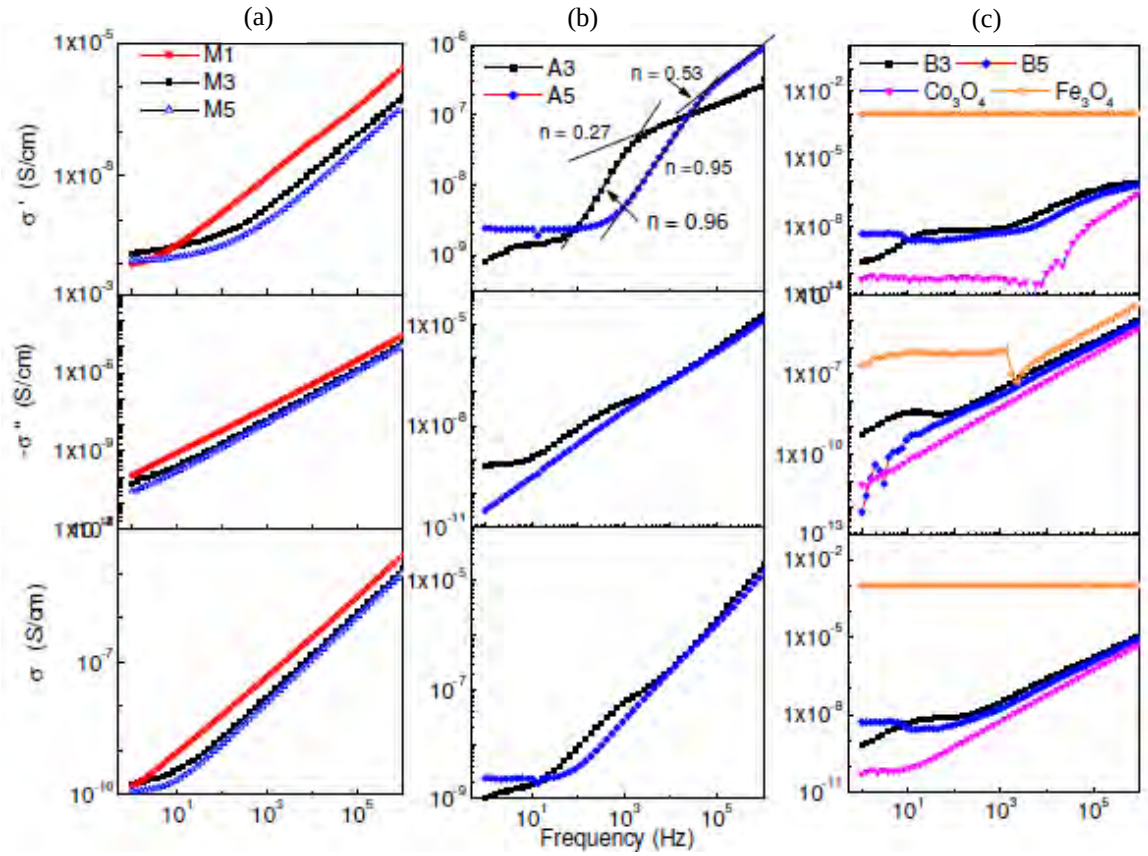

Figure 5. (Colour online) (log-log scale) Frequency dependence of ac conductivity (σ', σ'' and σ) at 1 Oe ac field for different samples at room temperature.

compound formation, are drastically different in comparison with the milled samples, which represent the mixture of two spinels. The striking difference is that plateau like response clearly increases for higher Co content (x = 0.5) and indicated from the frequency response of $\sigma^{/}$ and σ. The $\sigma^{//}$ (absorption component of ac conductivity) shows more or less power law behaviour in the whole frequency range and significantly affecting the frequency response of the σ. The interesting feature is that $\sigma^{/}$ (dispersion scattering component) is showing two different frequency zones. Above the low frequency plateau, the $\sigma^{/}$ increases with larger power exponent and then, slowly increases (i.e., saturation type character) with low power exponent. Similar feature has been noted in many compounds (Jung, 2008). The frequency dependent ac conductivity of annealed (A3 and A5) samples is also reproduced in bulk (B3 and B5) samples, except the low frequency plateau region is further increased in bulk (B3 and B5) samples. We have compared the ac conductivity of highly conducting Fe_3O_4 and poor (semi) conducting Co_3O_4 spinels with the feature of B3 and B5 samples in Figure 5(c). We are confirmed that not only magnitude of ac conductivity, but also feature (i.e., low frequency plateau, saturation type character at higher frequencies) can be manipulated according to the doping of Co in Fe_3O_4 matrix. This experimental result is highly useful for designing application oriented materials with desired range of conductivity.

Figure 6 shows the Cole-Cole (imaginary part of the complex impedance: $Z^{//}$ vs. real part of the complex impedance: $Z^{/}$) plot for milled samples (Figure 6(a)), annealed samples (Figure 6(b)) and bulk samples (Figure 6(c)). The milled samples indicated a single semi-circle in Cole-Cole plot within the range of measurement frequency. By fitting the data using single semi-circle, we have calculated grain boundary resistance (R_{gb}) from the intercept of the fitted curve on the $Z^{/}$ axis at lower frequency side (i.e., higher value of $Z^{/}$ axis) and also grain boundary resistivity (ρ_{gb}) by incorporating the dimension of the sample. Figure 6(b) shows a typical estimation of R_{gb} for A5 sample. The linear increase of $Z^{//}$ vs. $Z^{/}$ at lower frequency side (i.e., higher value of $Z^{/}$ axis) for A3 sample arises due to the electrode effect. Similar feature was observed in other compounds (Sivakumar *et al.*, 2007). The bulk samples also give the signature of a single semi-circle, although B3 samples showed an incomplete semi-circle. The interesting feature is that another semi-circle appeared at higher frequency side (i.e., lower value of $Z^{/}$ axis) for annealed and bulk samples (shown as inset in Figure 6(b) and Figure 6(c)). This is the contribution from highly conducting part of the sample, which is assumed to be grains in the spinel ferrite (Sivakumar *et al.*, 2007). In this case, electrical charge transport is controlled by the highly conductive grains and poor (semi) conducting grain boundary regions of the material. As shown in Table 1, the grain boundary resistivity (ρ_{gb}) for M1 sample is significantly higher in comparison with M3 and M5 samples where partial alloying at the grain boundary of the two starting spinels was indicated from the XRD and FTIR data. On the other hand, annealed and bulk

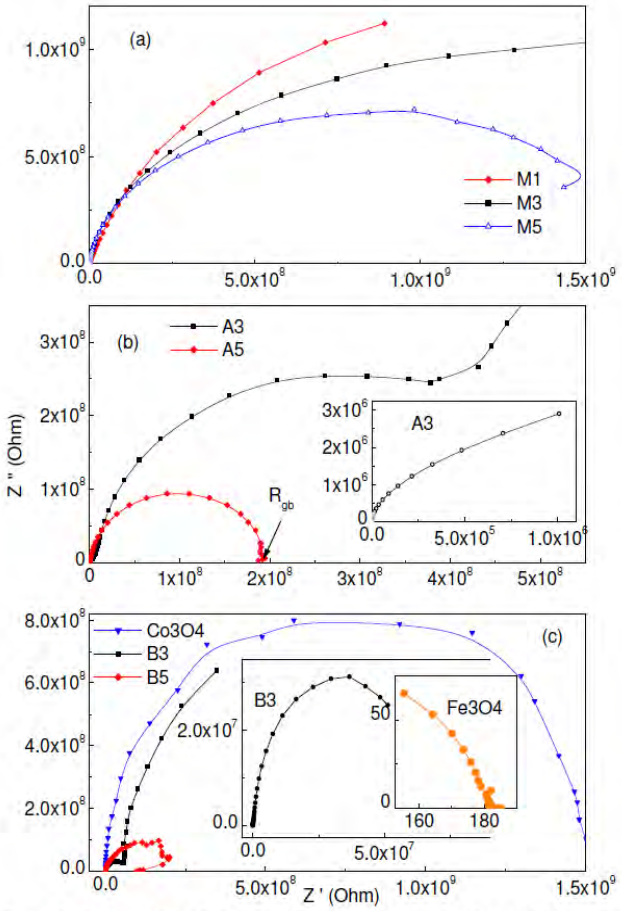

Figure 6. (Colour online) Col-Col plot for different samples. Inset of (b) and (c) shows the signature of second semi-circle due to grains at higher frequencies.

samples have shown a general tendency of decreasing ρ_{gb} with the increase of Co content. This is a typical example of the conductivity modulation at the grain boundaries of highly conductive Fe_3O_4 (ρ_{gb} ~ 590 Ohm-cm) and poor (semi) conducting Co_3O_4 spinels (15.69X10^9 ohm-cm). We noted from Table 1 that grain resistivity (ρ_g) of A5 sample is slightly low in comparison with A3 sample, where as (ρ_g) of B5 sample is slightly higher than B3 sample. This means conductivity of the grains decreases with the increase of Co for bulk samples. This may be expected due to increasing fraction of poor conducting Co_3O_4 spinels. On the other hand, nano-sized grains become more conductive with the increase of Co content for mechanical alloyed and subsequent annealing samples. A detailed analysis of the grain and grain boundary contribution of the samples at different temperatures will be studied in future work.

Figure 7 shows the variation of complex permittivity (real: ε', imaginary: ε'', absolute permittivity: ε) with frequency. We noted that there is a remarkable enhancement of dielectric permittivity in the annealed (Figure 7 (b)) and bulk samples (Figure 7(c)) in comparison with the milled (Figure 7(a)) samples. Among the milled samples, the permittivity (ε', ε'', ε) of A1 sample slowly decreases through out the frequency range. However, M3 and M5 samples showed a rapid decrease of the permittivity within 100 Hz and then, slowly decreases with the increase of frequency up to 1 MHz. It may be noted that there is a signature of slope change in the ε'' vs. frequency curve at about 5 kHz and 20 kHz for M1 and M3 samples, respectively, and ε'' is continuously decreasing with frequency. On the other hand, there is a sharp increase of ε' below 10 Hz, a plateau type region of ε' in the frequency range 10-1000 Hz, and a sharp decrease of ε' above 1000 Hz is followed by second plateau type region of ε'(f) for A3 sample. This typical feature has been observed in multiferroic (ferroelectric + magnetic) materials (Viviani *et al*., 2009). The ε'(f) of A5 sample showed plateau type behavior up to 5 kHz, then decreases slowly up to frequency 100 kHz and another plateau type region appears above 100 kHz. In the absorption component of complex permittivity (ε''), we noted a significant increase at lower frequency and magnitude wise ε'' is comparable (for A3 sample) or larger (for A5 sample) than the value of ε'' (say at 1 Hz). A relaxation peak in the ε''(f) curve was noted at about 1 kHz for A3 sample and 45 kHz for A5 sample, respectively. The shape of ε (f) curve suggests that dispersion of dielectric permittivity is strongly affected by the absorption component (ε''). If we look at the dispersion curve of bulk samples (Figure 7(c)), the ε'' (f) curve is nearly identical to that of A3 and A5 samples, except the peaks are little bit broad at about 37 kHz and 40 kHz for B 3and B5 samples, respectively. Otherwise, there is no significant change in

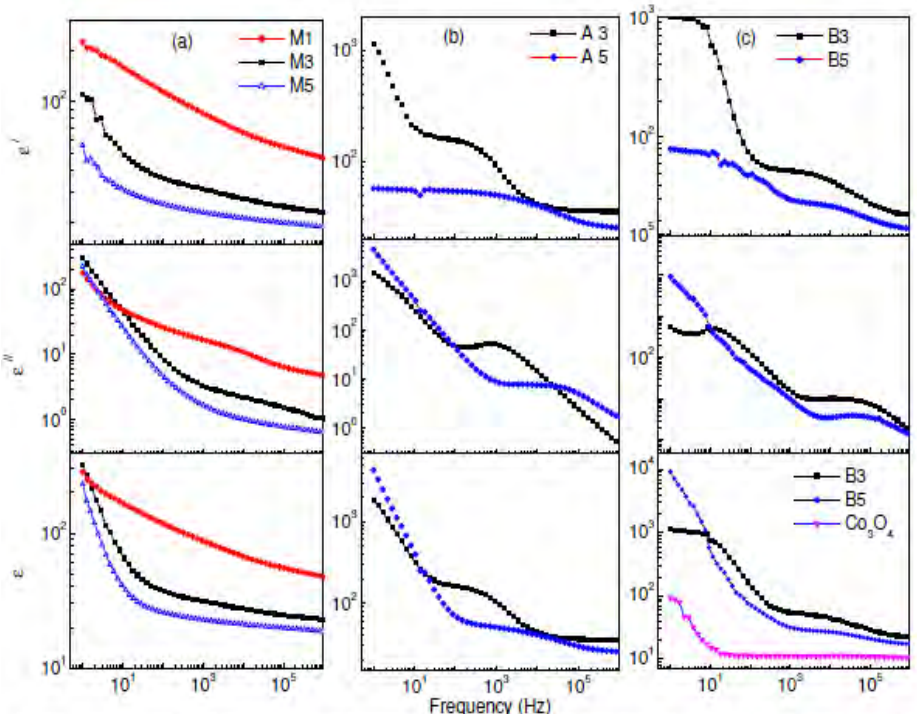

Figure 7. (Variation of room temperature ε', ε'' and ε with frequency at 1 ac volt for different samples.

the nature of frequency dependence of ε' and ε of bulk samples in comparison with annealed samples. The broad relaxation peak in the present composite material is not consistent with a typical Debye type single relaxation process in the material (Hill and Dissado,1985). Rather a distribution of dielectric component is expected, which can be attributed due to the inter-facial polarization at the grain and grain boundary of the composite material and can be explained on the basis of Maxwell-Wagner model and Koop's theory (Gopalan *et al*., 2008; Miles *et al*.,1957; Viviani *et al*., 2009).

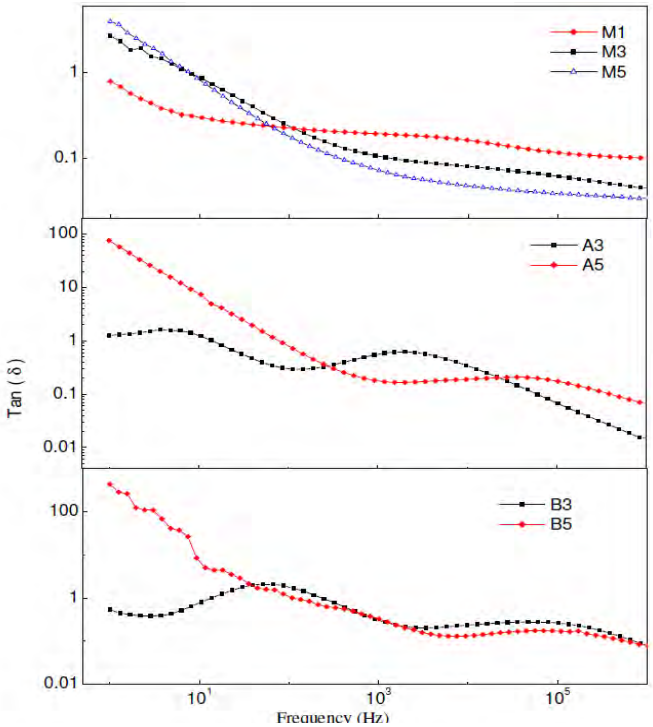

Figure 8. Variation of dielectric loss (tanδ) with frequency at 1 ac voltage for different samples.

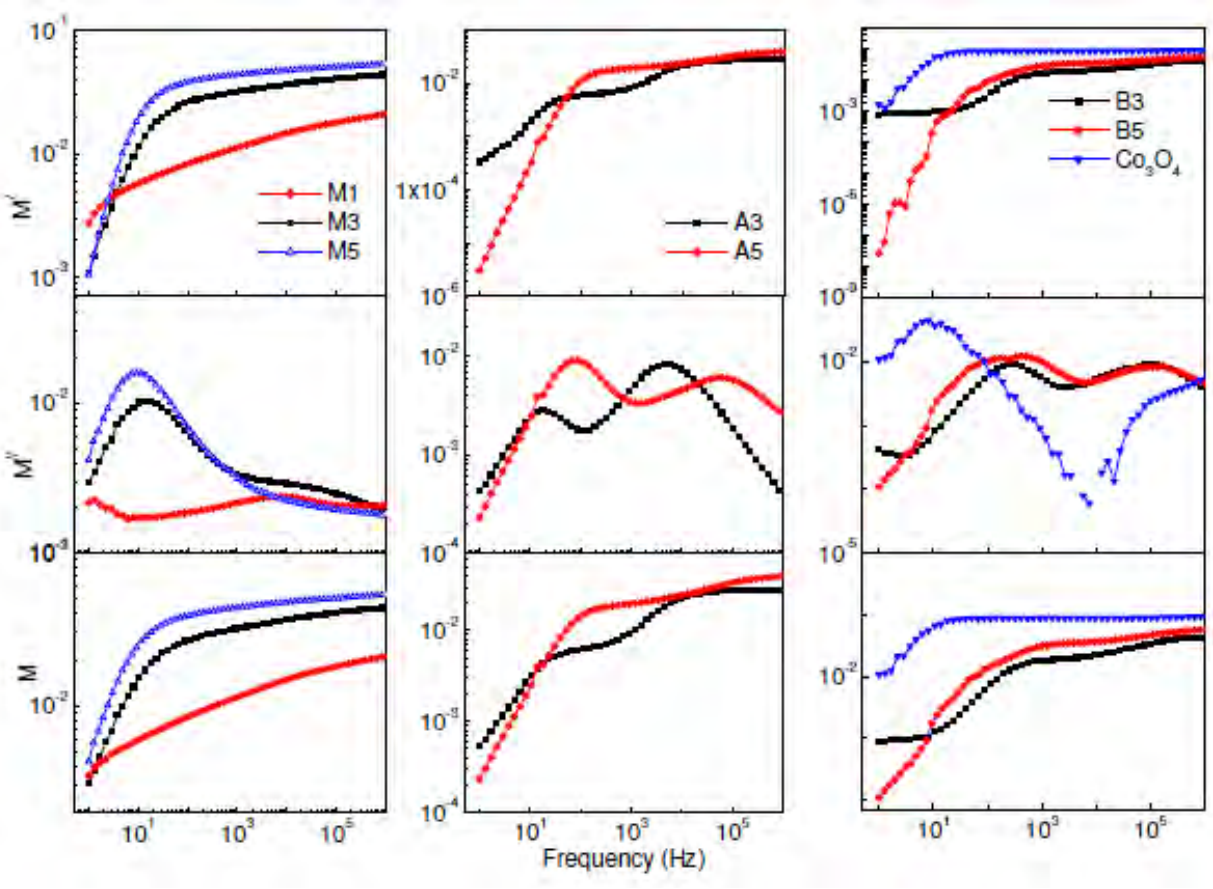

Figure 9. Variation of $M^{/}$, $M^{//}$ and M with frequency at 1 ac voltage for different samples.

The interesting feature is that dielectric constant (ε) of the bulk materials is not only significantly large in comparison with Co_3O_4 sample, but also comparable to many Co based multiferroic spinels (Meena *et al*., 2009). The coexistence of at least two dielectric components, one from grains and another from grain boundaries, in the annealed and bulk samples of the present composition is further indicated from two peaks in the frequency dependence of dielectric loss (tanδ) (in Figure 8) and electric modulus (real: $M^{/}$, imaginary: $M^{//}$, and resultant: M) (in Figure 9). Dielectric relaxation is strongly reflected in the imaginary component of Modulus ($M^{//}$). It may be noted that relaxation feature (more like a single relaxation process) of milled samples is significantly different in comparison with the annealed and bulk samples. This means the dielectric dynamics of milled samples, where two spinel phases are coexisting in each other, are drastically different from the samples where Co atoms are being incorporated in the spinel lattices of $Fe_{3(1-x)}Co_{3x}O_4$ composition. The mechanism of electrical conduction and multiferroelectricity in the present materials may be controlled by many factors in spinel lattices, e.g., site exchange among A and B sites cations, exchange of electrons among B site cations ($Fe^{2+} \leftrightarrow Fe^{3+}$, $Co^{3+} \leftrightarrow Co^{2+}$), interfacial interaction between grain and grain boundary spin, structural disorder at the interfaces (grain boundaries) of grains and grain size effects, effects of magnetic domain and magnetic disorder (Gopalan *et al*., 2008; Meena *et al.*, 2009; Mitsuda *et al*., 2010; Heikes *et al.*, 1957). It is believed that at lower frequency region the grain boundaries are more active and hopping between ions Fe^{3+} and Fe^{2+} is less. As the frequency increases the conductive grain becomes more active and also hopping between $Fe^{3+} \leftrightarrow Fe^{2+}$ and $Co^{2+} \leftrightarrow Co^{3+}$ on octahedral sites activates (Heikes *et al*., 1957; Farea *et al.*, 2008; Jonker *et al*., 1959).

4. Conclusions

The composite of $Fe_{3(1-x)}Co_{3x}O_4$ spinel ferrite (x = 0.1, 0.3 and 0.5) has been synthesized by mechanical alloying of highly conducting Fe_3O_4 and poor (semi)conducting Co_3O_4, and subsequent annealing at 950^0C. The crystalline phase and basic dielectric properties of annealed samples are well matched to the features of bulk samples that were prepared at high temperature solid state sintering. We found that single phased cubic spinel structure is not completely formed for the lower value of Co content in the present composition; otherwise crystal phase is well stabilized in a cubic spinel structure for higher value of Co content. The incorporation of Co in the lattices of Fe_3O_4 has shown a remarkable increase of dielectric permittivity in the composition. We have also noted a systematic modification of electrical conductivity with the increase of Co content. Dielectric properties of the Co

doped samples are controlled by both grain and grain boundary kinetics. Dielectric properties are assumed to be affected by the exchange of cations between tetrahedral (A) and octahedral (B) sites and hopping of holes ($Co^{3+} \rightarrow Co^{2+}$) and electrons ($Fe^{2+} \rightarrow Fe^{3+}$) among B site cations. This is a typical magnetic composite whose experimental results are interesting for the understanding of the connectivity between structural phase heterogeneity and physical properties. This work also provides the insight of the mechanism played by lattice disorder and spins at the interfaces (grain boundary) of two grains. Details of the ac conductivity and dielectric properties, and magnetic study are on progress to explore the multi-functionalities of these reported samples.

Acknowledgement: The authors thank to CIF, Pondicherry University for providing experimental facilities. RNB also thanks to UGC for financial support [F.NO. 33-5/2007 (SR)].

References

Chicinas I., 2006. Soft magnetic nanocrystalline powders produced by mechanical alloying routes. *Journal of Optoelectronics and Advanced Materials*, Vol.8, No.2, 439-448.

Fannin P.C., Marin C.N., Malaescu I., Stefu N., 2007. An investigation of the microscopic and macroscopic properties of magnetic fluids. *Physica B: Condensed Matter*, Vol.388, pp. 87-92.

Farea A.M.M., Kumar S., Batoo K.M., Yousef A., Alimuddin, 2008. Influence of frequency, temperature and composition on electrical properties of polycrystalline $Co_{0.5}Cd_xFe_{2.5-x}O_4$ ferrites. *Physica B: Condensed Matter*, Vol.403, pp. 684-701.

Franco Jr A.., and Zapf V., 2008. Temperature dependence of magnetic anisotropy in nanoparticles of $Co_xFe_{(3-x)}O_4$. *Journal of Magnetism and Magnetic Materials*, Vol.320, Issue 5, pp. 709-713.

Garc´ıa J., and Sub´ıas G., 2004. The Verwey transition-a new perspective. *Journal of Physics: Condensed Matter*, Vol.16, pp. R145-R178.

Gopalan E.V., Malini K.A., Saravanan S., Kumar D.S., Yoshida Y. and Anantharaman M.R., 2008. Evidence for polaron conduction in nanostructured manganese ferrite. *Journal of Physics D: Applied Physics*, Vol. 41, pp. 185005-9.

Heikes R.R., Johnson W.D., 1957. Mechanism of Conduction in Li-Substituted Transition Metal Oxides. *Journal of Chemical Physics*, Vol 26, Issue. 3, pp. 582-587.

Hill R.M. and Dissado L.A., 1985. *Journal of Physics C*: *Solid State Physics*. Vol.18, pp. 3829-3836.

Huang D.J., Lin H.-J., Okamoto J., Chao K.S., Jeng H.-T., Guo G.Y., Hsu C.-H., Huang C.-M., Ling D.C., Wu W.B., Yang C.S., and Chen C.T., 2006. Charge-Orbital ordering and verwey transition in magnetite measured by resonant Soft X-Ray Scattering. *Physical Review Letters*. Vol.96, pp. 096401-4.

Jonker G.H., 1959. Analysis of the semiconducting properties of cobalt ferrite. *Journal of Physics and Chemistry of Solids*, Vol.9, pp. 165-175.

Jun Y.-wook, Choi J.-sil, and Cheon J. 2007. Heterostructured magnetic nanoparticles: their versatility and high performance capabilities. *Chemical Communications*, Vol. 1203, 1203–1214.

Jung W.H., 2008. AC conduction mechanisms of $Gd_{1/3}Sr_{2/3}FeO_3$ ceramic. *Physica B, Condensed Matter*, Vol.403, pp. 636-638.

Kim K.J., Kim H.K., Park Y.R., Ahn G.Y., Kim C.S., and Park J.Y., 2006. Mössbauer and optical investigation of $Co_{3-x}Fe_xO_4$ thin films grown by sol-gel process. *Hyperfine Interactions*, Vol.169, pp. 1363-1369.

Li J.H., Hong R.Y., Li H.Z., Ding J., Zheng Y., Wei D.G., 2009. Simple synthesis and magnetic properties of $Fe_3O_4/BaSO_4$ multi-core/shell particles. *Materials Chemistry and Physics*, Vol. 113 , pp. 140-144.

Li Wen-hui, 2008. Microwave-assisted hydrothermal synthesis and optical property of Co_3O_4 nanorods. *Materials Letters*, Vol.62, pp. 4149-4151.

Meena P.L., Kumar R., Prajapat C.L., Screenivas K., and Gupta V., 2009. Dielectric studies of $Co_{3-x}Mn_xO_4$ (x = 0.1 – 1.0) cubic spinel multiferroic. *Journal of Applied Physic*, Vol.106, pp. 024105-6.

Miles P.A., Westphal W.B., and Hippel V.A., 1957. Dielectric spectroscopy of ferromagnetic semiconductors. *Reviews of Modern Physics*, Vol.29, No.3, pp. 279-307.

Mitsuda S., Yamano M., Kuribara K., Nakajima T., Masuda K., Yoshitomi .K, Terada .N, Kitazawa .H, Takenaka .K and Takamasu .T, 2010. Dielectric relaxation in a nonferroelectric phase of magneto-electric multiferroic $CuFeO_2$, *Journal of Physics, Conf. Ser.Vol.* 200, pp 012120.

Muthuselvam I.P., Bhowmik R.N., 2010. Mechanical alloyed Ho^{3+} doping in $CoFe_2O_4$ spinel ferrite and understanding of magnetic nanodomains. *Journal of Magnetism and Magnetic Materials*, Vol.322, pp. 767-776.

Ramos A.V., Moussy J.-B., Guittet M.-J., Gautier-Soyer M., Gatel C., Bayle-Guillemaud P., Warot-Fonrose B., and Snoeck E., 2007. Influence of a metallic or oxide top layer in epitaxial magnetic bilayers containing $CoFe_2O_4$ (111) tunnel barriers. *Physical Review B*, Vol.75, pp. 224421-8.

Sivakumar N., Narayanasamy A., Shinoda K., Chinnasamy C.N., Jeyadevan B., and Greneche J.-M., 2007. Electrical and magnetic properties of chemically derived nanocrystalline cobalt ferrite. *Journal of Applied Physics*, Vol.102, Issue 1, pp. 013916-013923.

Tseung A.C.C., Goldstein T.R., 1972. The preparation and characterization of ultrafine cobalt-iron oxides. *Journal of Material Science*, Vol.7, pp. 1383-1390.

Virden A., Wells S., Grady K.O., 2007. Physical and magnetic properties of highly anisotropic cobalt ferrite particles. *Journal of*

Magnetism and Magnetic Materials, Vol.316, pp. e768-771.
Viviani M., Bassoli M., Buscaglia V., Buscaglia M.T., and Nanni P., 2009. Giant permittivity and Maxwell-Wagner relaxation in Yb:$CaTiO_3$ ceramics. *Journal of Physics D: Applied Physics*, Vol.42, pp. 175407-8.
Wang W.D., Yu M.H., Chen Y.X., and Tang J.K., 2006. Large room-temperature spin-dependent tunneling magneto resistance in a Fe_3O_4 polymer composite system. *Journal of Applied Physics*, Vol.99, pp. 08J108-3.
Waldron R.D., 1955. Infrared spectra of ferrites. *Physical Review*. Vol.99, pp. 1727-1735.

Biographical notes:

R.N. Bhowmik, M.Sc. and Ph.D. in Physics, is the Assistant Professor in the Department of Physics, Pondicherry University, India. He is one of the leading Scientists in the Condensed Matter research group in Pondicherry University. Dr. Bhowmik is also associated with four international journals for reviewing the research papers. He is working on different types of magnetic oxides, including spinel ferrites, perovskites, double perovskites, transition metal based oxides and magnetic nanocomposite. His main research interest is to study magnetic, magneto-transport and dielectric properties of magnetic, electronic and multiferroic materials.

N. Naresh, M.Sc. and M.Phil in Physics, is currently continuing his doctoral degree in the department of Physics, Pondicherry University. He is working on the transition metal doped hematite and magnetic composite materials.

Received August 2010
Accepted October 2010
Final acceptance in revised form October 2010